A Nonlinear Distributed Control Strategy for a DC MicroGrid using Hybrid Energy Storage for Voltage Stability

Filipe Perez, Gilney Damm, Paulo Ribeiro, Françoise Lamnabhi-Lagarrigue, Lilia Galai-Dol

A Nonlinear Distributed Control Strategy for a DC MicroGrid using Hybrid Energy Storage for Voltage Stability

Filipe Perez, Gilney Damm, *Member, IEEE*, Paulo Ribeiro, *Fellow, IEEE*
Françoise Lamnabhi-Lagarrigue, Lilia Galai-Dol

***Abstract*— DC MicroGrids with the integration of renewable energy sources (renewables) and energy storage systems can improve the performance of power systems, ensuring safe operation of a local network, where the MicroGrid control is responsible to assure stability and power quality of the system. This paper proposes a distributed nonlinear control strategy for a DC MicroGrid composed of a PV, a battery storage and a supercapacitor to properly supply a local AC load, where a complete stability analysis in conducted using Lyapunov techniques. The MicroGrid is connected to an AC grid by a VSC converter, which injects the right amount of active and reactive power according to the AC load demand. The supercapacitor's duty is to control DC bus voltage dealing with transient stability while the battery fulfills long term power flow, where the energy is controlled to assure power flow balance, ensuring proper operation for the MicroGrid. Simulation results illustrate the performance of the proposed control and the system's operation.**

I. Introduction

The advantages of DC MicroGrids has been highlighted in many studies over the years. First, because recent devices based on power electronics: modern loads, renewables and energy storage are intrinsically DC. Therefore, the converters topology and the control strategy required in these systems are much simpler. Besides that, energy efficiency is also improved and the system is much easier to deal with since reactive power, frequency regulation, synchronization and power factor are not a problem anymore. Renewables can also be better integrated since the intermittent aspect is eliminated when coupled with energy storage systems. All of these reasons have brought DC MicroGrids as a new trend in the electrical grid modernization [1], [2], [3].

A great challenge of MicroGrids is to develop a control strategy to assure stable and reliable operation of the system, such that the balance of generation and consumption is regulated, stabilizing their fundamental states. When the MicroGrid is grid-connected, it is possible to inject/absorb arbitrary amounts of power to the AC side for ancillary services purposes or even to supply a local load, therefore the synchronization is required for this operation mode, but frequency, angle and inertia problems are dealt by the main network [4], [5].

In several papers, a linear control strategy is proposed to operate a MicroGrid, but a rigorous stability analysis is usually out of scope in this kind of study, where just a small operating region is considered. As a MicroGrid needs to operate in a wide region, with different sets of operation's parameters, a more robust control strategy is necessary. Therefore, the nonlinear control approach becomes more evident for a MicroGrid application, where a more rigorous stability study can be developed [6], [7], [8]. The nonlinear control allows the system to work in a broader region of operation, justifying the use of a more complex approach. Also, a distributed approach as the one developed in this work, allows independent operation of each device in system assuring greater flexibility and improving reliability, against the centralized strategy where a communication fail can bring down the whole system [9], [10], [11]. Indeed, the proposed control strategy is said distributed because the control laws are developed for each converter connected to the DC grid, only using local measurements and references given by higher level controllers [12], [13].

This paper proposes a distributed nonlinear control strategy for a DC MicroGrid in order to properly supply a local AC load, assuring power flow balance and stabilization in the DC bus voltage of the MicroGrid. The energy storage system of the MicroGrid is composed by a hybrid topology, where two distinct technologies are applied to work in different time-scales. The supercapacitor is chosen to regulate the DC bus voltage responding to fast-transient disturbances, and the battery provides the power flow balance in a slower time-scale, assuring proper operation in the MicroGrid. Dynamic feedback linearization is applied on the supercapacitor subsystem based on a explicit time-scale separation, where singular perturbation analysis is done. This approach solves the minimum-phase problem of boost converters according to the chosen control target. A rigorous stability analysis is developed by Lyapunov techniques assuring stability of the whole grid, resulting in Input-to-State Stability (ISS) property. Detailed simulations on circuit level using *SimPowerSystem* toolbox from *Matlab/Simulink* shows the behavior of the proposed control law.

The paper is organized as follows: Section II introduces the considered MicroGrid model, Section III describes the adopted control strategy, simulations results are introduced in Section IV and conclusions are provided in Section V.

Filipe Perez and Françoise Lamnabhi-Lagarrigue are with L2S laboratory, Paris-Saclay University, 3 rue Joliot Currie, Gif-Sur-Yvette, France, filipe.perez@l2s.centralesupelec.fr

Gilney Damm is with IBISC Laboratory, Paris-Saclay University, 43 Rue du Pelvoux, Courcouronnes, France, gilney.damm@ibisc.fr

Paulo F. Ribeiro and Filipe Perez are with ISEE, Federal University of Itajubá, 1303 Av. BPS, Itajubá, Brazil, pfribeiro@ieee.org

Lilia Galai-Dol and Gilney Damm are with Efficacity, R&D Center, Paris, France, l.galai-dol@efficacity.com

II. MicroGrid Model

In this paper, it is developed a grid-connected DC MicroGrid composed by a supercapacitor, a battery, a PV array as the main power generation and an AC load connected to the point of commom coupling (PCC). The AC load must be properly supplied inside of grid requirements. The supercapacitor and the battery work in different time-scales acting in a complementary way to guarantee grid stability. Fig. 1 introduces the proposed MicroGrid. The dynamic equations of the DC MicroGrid is written as follows.

$$\dot{V}_{C_1} = \frac{1}{R_1 C_1} V_S - \frac{1}{R_1 C_1} V_{C_1} - \frac{1}{C_1} I_{L_3} \quad (1)$$

$$\dot{V}_{C_2} = \frac{1}{R_2 C_2} V_{dc} - \frac{1}{R_2 C_2} V_{C_2} + \frac{1}{C_2} I_{L_3}(1-u_1) \quad (2)$$

$$\dot{I}_{L_3} = \frac{1}{L_3} V_{C_1} - \frac{1}{L_3} V_{C_2}(1-u_1) - \frac{R_{01}}{L_3} I_{L_3} \quad (3)$$

$$\dot{V}_{C_4} = \frac{1}{R_4 C_4} V_B - \frac{1}{R_4 C_4} V_{C_4} - \frac{1}{C_4} I_{L_6} \quad (4)$$

$$\dot{V}_{C_5} = \frac{1}{R_5 C_5} V_{dc} - \frac{1}{R_5 C_5} V_{C_5} + \frac{1}{C_5} I_{L_6}(1-u_2) \quad (5)$$

$$\dot{I}_{L_6} = \frac{1}{L_6} V_{C_4} - \frac{1}{L_6} V_{C_5}(1-u_2) - \frac{R_{04}}{L_6} I_{L_6} \quad (6)$$

$$\dot{V}_{C_7} = \frac{1}{R_7 C_7} V_{PV} - \frac{1}{R_7 C_7} V_{C_7} - \frac{1}{C_7} I_{L_9} \quad (7)$$

$$\dot{V}_{C_8} = \frac{1}{R_8 C_8} V_{dc} - \frac{1}{R_8 C_8} V_{C_8} + \frac{1}{C_8} I_{L_9}(1-u_3) \quad (8)$$

$$\dot{I}_{L_9} = \frac{1}{L_9} V_{C_7} - \frac{1}{L_9} V_{C_8}(1-u_3) - \frac{R_{08}}{L_9} I_{L_9} + \\ + \frac{1}{L_9}(R_{08} - R_{07}) I_{L_9} u_3 \quad (9)$$

$$\dot{I}_{ld} = -\frac{R_l}{L_l} I_{ld} + \omega I_{lq} + \frac{1}{2L_l} V_{C_{11}} u_4 - \frac{V_{ld}}{L_l} \quad (10)$$

$$\dot{I}_{lq} = -\frac{R_l}{L_l} I_{lq} - \omega I_{ld} + \frac{1}{2L_l} V_{C_{11}} u_5 - \frac{V_{lq}}{L_l} \quad (11)$$

$$\dot{V}_{C_{11}} = \frac{(V_{dc} - V_{C_{11}})}{R_{11} C_{11}} - \frac{3}{2} \frac{V_{ld} I_{ld} + V_{lq} I_{lq}}{C_{11} V_{C_{11}}} \quad (12)$$

$$\dot{V}_{dc} = \frac{1}{C_{10}} \left[\frac{1}{R_2}(V_{C_2} - V_{dc}) + \frac{1}{R_5}(V_{C_5} - V_{dc}) + \right. \\ \left. + \frac{1}{R_8}(V_{C_8} - V_{dc}) + \frac{1}{R_{11}}(V_{C_{11}} - V_{dc}) \right] \quad (13)$$

V_{dc} is the DC bus voltage, V_S, V_B and V_{PV} are the voltages on the supercapacitor, battery and PV array respectively. V_{C_1}, V_{C_4} and V_{C_7} are the input voltages of the MicroGrid converters. I_{L_3}, I_{L_6} and I_{L_9} are the inductor currents in the converters, V_{C_2}, V_{C_5}, V_{C_8} and $V_{C_{11}}$ are the output voltages of the converters. I_{ld} and I_{lq} are the AC currents in dq frame, V_{ld} and V_{lq} are the respective voltages of the AC grid in dq frame, where $\omega = 2\pi f_l$ is the grid frequency. R_l and L_l are the line impedance of the AC grid. R_1, R_2, R_4, R_5, R_7, R_8 and R_{11} are the resistances representing the cable losses, R_{01}, R_{02}, R_{04}, R_{05}, R_{07} and R_{08} are switch losses of the semiconductors and u_1, u_2, u_3, u_4 and u_5 are the modulation index of the converters in the MicroGrid.

The supercapacitor target is to control the voltage V_{dc} on the DC bus to provide transient stability (in milliseconds) in the system. In this case, a control strategy is developed to control the DC bus based on a Lyapunov function that assures stability for the whole system. A bidirectional-boost converter is applied for the supercapacitor subsystem, where the existing non-minimal phase problem is solved here by using dynamical feedback linearization control strategy. Voltage V_{C_2} is controlled such that V_{dc} is stabilized [2], [9], [8]. The supercapacitor equations are introduced in (1)-(3).

A battery bank is used to balance the grid power flow in a slower time-scale (seconds to minutes), where the current I_{L_6} is driven to reference $I^*_{L_6}$, such that the battery regulates the energy mismatch in the system. The reference $I^*_{L_6}$ is calculated by the secondary controller taking into account weather and load prediction and the state of charge (SoC) of the energy storage elements using optimization techniques [14]. A bidirectional-boost converter is applied in the battery subsystem and the equations are introduced in (4)-(6).

The PV array is controlled to inject the maximum available power into the grid. The current I_{L_9} follows the reference $I^*_{L_9}$, which is given by a MPPT algorithm such that the PV target is accomplished [10]. The MPPT can be included in the secondary control. The PV equations are introduced in (7)-(9), where a boost converter is used.

The grid-connection is made by a VSC converter, where an AC load must be supplied by the DC MicroGrid. The AC grid equations are introduced in (10)-(12). The control target is to correctly supply the AC load by injecting the right amount of active P^* and reactive Q^* power into the AC grid [15]. This target is accomplished by directly controlling the currents I_{ld} and I_{lq}, since their references can be obtained by:

$$I^*_{ld} = \frac{2}{3}\frac{P^*}{V_{ld}}, \qquad I^*_{lq} = \frac{2}{3}\frac{Q^*}{V_{ld}} \quad (14)$$

The dynamic equation of the voltage DC bus is introduced in (13) and it represents the connection of all devices in the DC MicroGrid. It is extremely important to control the DC bus voltage to assure proper operation of each device in the system. The DC bus voltage responds to power variations in the grid, and then a balanced DC bus voltage means power flow regulation. To accomplish this target the DC bus is controlled in a fixed reference V^*_{dc}.

This paper focus on the low level control strategy of the proposed MicroGrid, therefore it is assumed that there is a secondary controller that provides the references of battery current I_{L_6} such that long term power flow and the SoC of the storages are optimized. Second, it is considered that the MicroGrid was properly designed, where the PV, battery and supercapacitor were sized according to the AC load demand. The supercapacitor is specially sized according to the maximum power variation in the system.

III. Control Strategy

In the boost converter of the supercapacitor, the output voltage chosen as the control output results in non-minimal

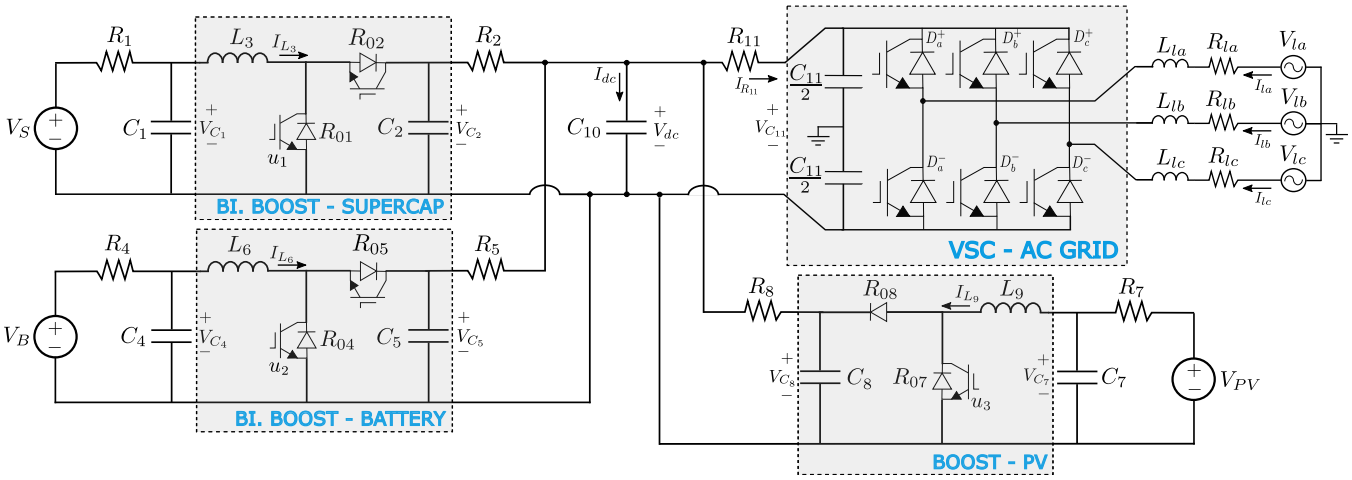

Fig. 1. The DC MicroGrid composed of a supercapacitor, a battery, a PV array and a load in AC grid connection.

phase behavior with unstable zero dynamics. Therefore, the control scheme is based on control induced time scale separation that artificially split into two subsystems with different time-scales. The first subsystem is composed by the current I_{L_3} in the supercapacitor's inductor, where the control gains are allocated to induce much fast dynamics than the second subsystem, which is composed by voltage V_{C_2}. The remaining systems in the MicroGrid (Battery, PV and AC grid) are first order systems controlled by feedback linearization.

A. Current controlled systems

Defining x as the state variables, x^e as the equilibrium points, the control output is y and u is the control input. This subsection presents the control of the currents in the MicroGrid:

$$y_1 = [I_{L_3}, I_{L_6}, I_{L_9}, I_{ld}, I_{lq}]^T \tag{15}$$

where $x_1^e = [I_{L_3}^e, I_{L_6}^*, I_{L_9}^*, I_{ld}^*, I_{lq}^*]^T$ are equilibrium points and the systems' disturbances are defined as follows:

$$d = [V_S, V_B, V_{PV}, V_{ld}, V_{lq}]^T \tag{16}$$

with $x_1 = [V_{C_1}, V_{C_4}, V_{C_5}, V_{C_7}, V_{C_8}, V_{C_{11}}]^T$ being the non-controlled dynamics.

Here, the control law of each device can be developed independently by feedback linearization technique, which is the result of the distributed approach, since each system has a different control target. It is possible to design a nonlinear feedback linearizing control input written as:

$$u_1 = 1 + \frac{1}{V_{C_2}}\left[L_3 v_3 - V_{C_1} + R_{01} I_{L_3}\right] \tag{17}$$

$$u_2 = 1 + \frac{1}{V_{C_5}}\left[L_6 v_6 - V_{C_4} + R_{04} I_{L_6}\right] \tag{18}$$

$$u_3 = \frac{L_9 v_9 - V_{C_7} + V_{C_8} + R_{08} I_{L_9}}{V_{C_8} - (R_{08} - R_{07}) I_{L_9}} \tag{19}$$

$$u_5 = \frac{2L_l}{V_{C_{17}}}\left[v_{i_d} + \frac{I_{ld}}{L_l} - \omega I_{lq} + V_{ld}\right] \tag{20}$$

$$u_6 = \frac{2L_l}{V_{C_{17}}}\left[v_{i_q} + \frac{I_{lq}}{L_l} + \omega I_{ld} + V_{lq}\right] \tag{21}$$

where $v_i = [v_3, v_6, v_9, v_{id}, v_{iq}]$ is the additional control designed such that a linear stable subspace is generated:

$$v_3 = \dot{I}_{L_3}^e - K_3(I_{L_3} - I_{L_3}^e) - K_3^\alpha \alpha_3 \tag{22}$$

$$v_6 = -K_6(I_{L_6} - I_{L_6}^*) - K_6^\alpha \alpha_6 \tag{23}$$

$$v_9 = -K_9(I_{L_9} - I_{L_9}^*) - K_9^\alpha \alpha_9 \tag{24}$$

$$v_{i_d} = -K_d(I_{ld} - I_{ld}^*) - K_d^\alpha \alpha_d \tag{25}$$

$$v_{i_q} = -K_q(I_{lq} - I_{lq}^*) - K_q^\alpha \alpha_q \tag{26}$$

The integral terms α_i, where $i = [3, 6, 8, d, q]$, ensure zero error in steady state and can be written as: $\dot{\alpha}_i = x_i - x_i^e$. The gains K_i and K_i^α are positive constants and can be calculated by pole allocation from linear theory [16], [8].

B. Voltage controlled system

Since voltage V_{C_2} on the supercapacitor system is artificially allocated by the control design to have slower dynamics compared with current I_{L_3}, explicit time-scale separation allows the singular perturbation analysis. Then, voltage V_{C_2} is now the output control of the system and the state I_{L_3} is considered already on its equilibrium point $I_{L_3}^e$. The DC bus is regulated by the supercapacitor to assure asymptotic stability of the whole system. By suitable allocation of gains, it is possible to design the current I_{L_3} to be much faster than voltage V_{C_2} resulting in an explicit time-scale separation. Therefore, the result is a simplified dynamic of V_{C_2} as follows [2]:

$$\dot{V}_{C_2} = \frac{1}{R_2 C_2}(V_{dc} - V_{C_2}) + \frac{I_{L_3}^e}{C_2 V_{C_2}}[V_{C_1} - R_{01} I_{L_3}^e] \tag{27}$$

The chosen control input is $v_d = \dot{I}_{L_3}^e$, which defines the dynamic feedback linearization approach, calculated such that $V_{C_2} \to V_{C_2}^*$. Then, the control input v_d can be found in

the second time-derivative of V_{C_2} as follows:

$$\ddot{V}_{C_2} = \frac{\dot{V}_{dc}}{R_2 C_2} - \dot{V}_{C_2}\left[\frac{1}{R_2 C_2} + \frac{V_{C_1} I^e_{L_3} - R_{01} {I^e_{L_3}}^2}{C_2 {V_{C_2}}^2}\right] + \frac{1}{C_2 V_{C_2}} I^e_{L_3} \dot{V}_{C_1} + \frac{1}{C_2 V_{C_2}}(V_{C_1} - 2R_{01} I^e_{L_3}) v_d \quad (28)$$

Therefore we have obtained full state transformation with no zero dynamics. The control input v_d is calculated such that V_{C_2} is stabilized to $V^*_{C_2}$, and is presented in (29):

$$v_d = \frac{V_{C_2}}{V_{C_1} - 2R_{01} I^e_{L_3}}\left[C_2 v_2 - \frac{\dot{V}_{dc}}{R_2} - \frac{I^e_{L_3}}{V_{C_2}}\dot{V}_{C_1} + \dot{V}_{C_2}\left(\frac{1}{R_2} + \frac{V_{C_1} I^e_{L_3} - R_{01} {I^e_{L_3}}^2}{{V_{C_2}}^2}\right)\right] \quad (29)$$

with: $v_2 = -K_2(\dot{V}_{C_2} - \dot{V}^*_{C_2}) - K^\alpha_2(V_{C_2} - V^*_{C_2})$. We can define the speed of convergence for V_{C_2}, allocating the design gains $(K_2,\ K^\alpha_2)$ by pole placement to get slower voltage dynamics for the simplified model [2], [7]. Since current $I^e_{L_3}$ can be easily computed as $I^e_{L_3} = \int v_d dt$, it was possible to design a control law to steer $I_{L_3} \to I^e_{L_3}$ such that V_{C_2} is stabilized toward V_{C_2}. Then, we can use V_{C_2} to control the Voltage on the DC bus (V_{dc}) by calculating a reference $V^*_{C_2}$ that results in $V_{dc} \to V^*_{dc}$. The calculation of $V^*_{C_2}$ and the stability analysis is done in next subsection.

Remark 1: The supercapcitor control strategy split voltage V_{C_2} and current I_{L_3} in two subsystems where singular perturbation analysis can be made to solve the non-minimum phase problem. This time-scale separation does not represent the natural dynamics of the whole system, but is artificially developed.

Remark 2: The control design of each system on the MicroGrid can be developed separately, since a System-of-Systems approach is applied and they are related only by the DC bus voltage V_{dc}, which interconnect the whole system.

C. Stability Analysis

The control law developed for each device can accomplish the control targets exposed in Section II. Hence, the stability study is necessary to investigate the behavior of the whole system in closed-loop considering the calculation of $V^*_{C_2}$ that impose the balance on the DC bus of the MicroGrid. In this case, the dynamics of the interconnected system is taking into account.

We may propose a Lyapunov function to design the reference for V_{C_2} such that V_{dc} is stabilized in V^*_{dc}. The Lyapunov function is composed by the interconnection voltages of the MicroGrid to consider stability of the non-controlled variables of the whole system [7].

$$W(x) = \frac{C_{10}}{2} V^2_{dc} + \frac{C_5}{2}(V_{C_5} - V^e_{C_5})^2 + \frac{C_8}{2}(V_{C_8} - V^e_{C_8})^2 + \frac{C_{11}}{2}(V_{C_{11}} - V^e_{C_{11}})^2 \quad (30)$$

The time derivative can be calculated as follows, where V_{C_2} is the degree of freedom used as the control input:

$$\dot{W}(x) = V_{dc}\left[\frac{1}{R_2}(V_{C_2} - V_{dc}) + \frac{1}{R_5}(V_{C_5} - V_{dc}) + \frac{1}{R_8}(V_{C_8} - V_{dc}) + \frac{1}{R_{11}}(V_{C_{11}} - V_{dc})\right] + (V_{C_5} - V^e_{C_5})\left[\frac{1}{R_5}(V_{dc} - V_{C_5}) + I_{L_6}(1 - u_2)\right] + (V_{C_8} - V^e_{C_8})\left[\frac{1}{R_8}(V_{dc} - V_{C_8}) + I_{L_9}(1 - u_3)\right] + (V_{C_{11}} - V^e_{C_{11}})\left[\frac{1}{R_{11}}(V_{dc} - V_{C_{11}}) - \frac{3(I_{ld}V_{ld} + I_{lq}V_{lq})}{2V_{C_{11}}}\right] \quad (31)$$

In order to obtain a stable behavior, we investigate the time derivative of $W(x)$ [16], where a desired stable expression for $\dot{W}(x)$ can be stated as:

$$\dot{W}(x) = -\frac{1}{R_2}(V^2_{dc} - {V^*_{dc}}^2) - \frac{1}{R_5}(V_{C_5} - V^e_{C_5})^2 - \frac{1}{R_8}(V_{C_8} - V^e_{C_8})^2 - \frac{1}{R_{11}}(V_{C_{11}} - V^e_{C_{11}})^2 \quad (32)$$

Therefore, a control input $V^*_{C_2}$ is obtained substituting (32) in (31) to result in a reference trajectory that stabilizes the DC bus of the MicroGrid.

$$V^*_{C_2} = \frac{R_2}{V_{dc}}\left\{\frac{1}{R_2}{V^*_{dc}}^2 - V_{dc}\left[\frac{1}{R_5}(V_{C_5} - V_{dc}) + \frac{1}{R_8}(V_{C_8} - V_{dc}) + \frac{1}{R_{11}}(V_{C_{11}} - V_{dc})\right] - (V_{C_5} - V^e_{C_5})\left[\frac{1}{R_5}(V_{dc} - V_{C_5}) + I_{L_6}(1 - u_2)\right] - (V_{C_8} - V^e_{C_8})\left[\frac{1}{R_8}(V_{dc} - V_{C_8}) + I_{L_9}(1 - u_3)\right] - (V_{C_{11}} - V^e_{C_{11}})\left[\frac{V_{dc} - V_{C_{11}}}{R_{11}} - \frac{3(I_{ld}V_{ld} + I_{lq}V_{lq})}{2V_{C_{11}}}\right] - \frac{(V_{C_5} - V^e_{C_5})^2}{R_5} - \frac{(V_{C_8} - V^e_{C_8})^2}{R_8} - \frac{(V_{C_{11}} - V^e_{C_{11}})^2}{R_{11}}\right\} \quad (33)$$

We can state that there exist functions $\underline{\alpha}, \overline{\alpha} \in K_\infty$ such that $\underline{\alpha}(|\tilde{x}|) \le W_{\tilde{x}}(\eta) \le \overline{\alpha}(|\tilde{x}|)$, which results in:

$$\dot{W}_{\tilde{x}}(\tilde{x}, V^*_{dc}) \le -\beta_{\tilde{x}}(|\tilde{x}|) + \gamma_{\tilde{x}}(|V^*_{dc}|) \quad (34)$$

with $\beta_{\tilde{x}}, \gamma_{\tilde{x}} \in K_\infty$.

The Lyapunov function in (30) results to be an ISS-like Lyapunov function, where V^*_{dc} is playing the role of a virtual input [17], [18], [19]. The resulted ISS property for the MicroGrid is enough to assure the correctly operation of the system: assuring robustness and bounded states in the system [18], [20].

IV. Simulation Results

The proposed grid-connected DC MicroGrid is implemented on *SimPowerSystem* of *Simulink* to study stability and the control performance of the nonlinear control strategy. The supercapacitor has 100 F of capacitance and internal resistance of 9 $m\Omega$, with 400 V of nominal voltage composed of 18 parallel cells and 4 series cells. The nominal power capacity of the supercapacitor is 2.45 kW. The battery is a lithium-ion technology with 180 kW/180 kWh of

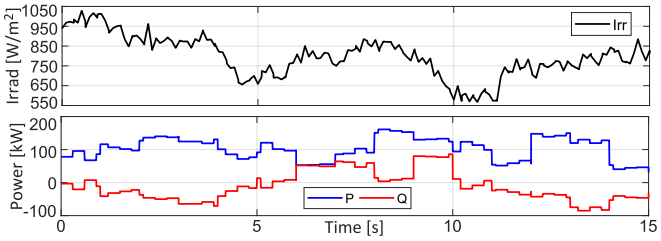

Fig. 2. Solar irradiation and load demand in AC grid.

capacity, 380 V of nominal voltage with 3.8 $m\Omega$ of internal resistance. This battery is allocated to have a piecewise constant variation to save its life cycle. The PV array is a monocrystalline Kyocera KC60 composed of 200 parallel cells and 15 series cells of 60 W, resulting in 180 kWp of power in the nominal conditions. The MPPT algorithm used is the incremental conductance one.

The AC grid has a line impedance of $L_l = 2\ mH$ and $R_l = 1\ m\Omega$, with short-circuit power of 10 MVA. The nominal frequency of the grid is $f_l = 50\ Hz$ and the rms voltage on the PCC is 220 V. An AC load with active and reactive power demand is connected in the PCC where the DC MicroGrid's target is to supply this AC load. The maximum power consumption of the AC load is 150 kW. The DC/DC converters work with 10 kHz of switching frequency and the VSC converter works with 20 kHz. Table I presents the DC MicroGrid parameters in the simulations.

TABLE I
MICROGRID PARAMETERS

Supercap	Battery	PV	AC Load	Value
R_1	R_4	R_7	R_{11}	0.1 Ω
C_1	C_4	C_7	C_{11}	10 mF
R_2	R_5	R_8	-	0.1 Ω
C_2	C_5	C_8	-	10 mF
L_3	L_6	L_9	-	3.3 mH
R_{01}	R_{04}	R_{07}	-	10 $m\Omega$
R_{02}	R_{05}	R_{08}	-	10 $m\Omega$

Fig. 2 introduces the incident irradiation on the PV panel and the demanded power for AC load. The irradiation and the active and reactive power demanded by the AC grid are the inputs for the simulation where the DC MicroGrid will operate according to these variable conditions. It is considered that the nonlinearities of these inputs can cause instability of the system justifying the choice of a nonlinear control strategy.

The voltages V_S, V_B and V_{PV} are depicted in Fig. 3. The supercapacitor voltage V_S varies to balance the power into the DC bus. The battery varies according to the second level control to provide power flow regulation. The PV voltage varies according to the irradiation profile.

Fig. 4 introduces the currents I_{L_3}, I_{L_6}, I_{L_9} and their respective control references. Here we can verify that supercapacitor works in fast transients to provide the DC bus stability, the reference current $I^*_{L_3}$ is continuously varying to correct the mismatch of power in the grid. The battery

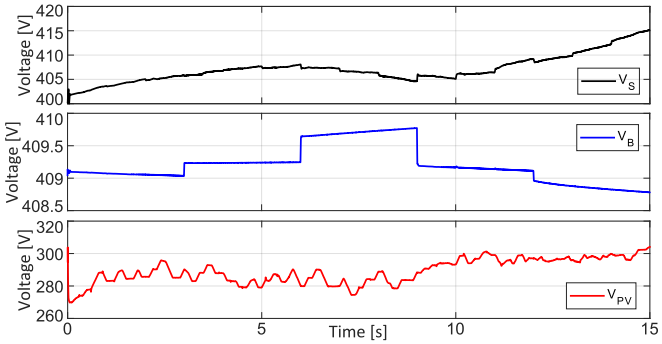

Fig. 3. Voltages V_S, V_B and V_{PV} respectively.

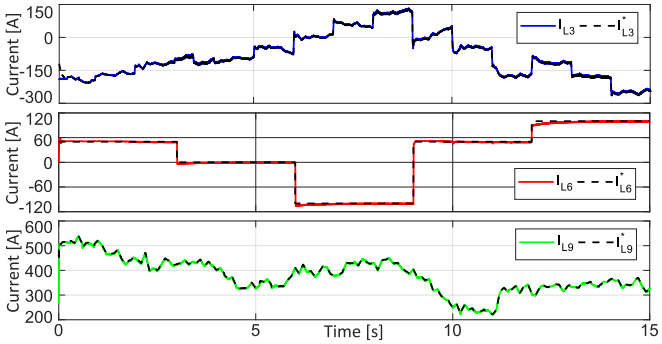

Fig. 4. Currents I_{L_3}, I_{L_6} and I_{L_9} respectively.

current I_{L_6} varies slowly following its reference calculated in the second level controller to balance the power flow in seconds to minutes. I_{L_6} tracks the maximum power point according to the incident irradiation on PV panel.

The voltage V_{C_2} is the control input selected in the supercapacitor subsystem to stabilize the DC bus voltage. The voltage on the DC bus V_{dc} is controlled in a constant reference $V^*_{dc} = 500\ V$, such that the balance of power is guaranteed, allowing each device of the system (Battery, PV and AC grid) operate according to their control targets. The voltage V_{dc} is properly controlled, presenting fast control response with good control performance. The voltages V_{C_2} and V_{dc} are depicted in Fig. 5.

The AC load requests active P^* and reactive Q^* power from the DC MicroGrid, then a reference is generated by the second control level where the currents I_{ld} and I_{lq} is controlled to accomplish this target. Therefore, the active and reactive power are supplied into AC grid as presented

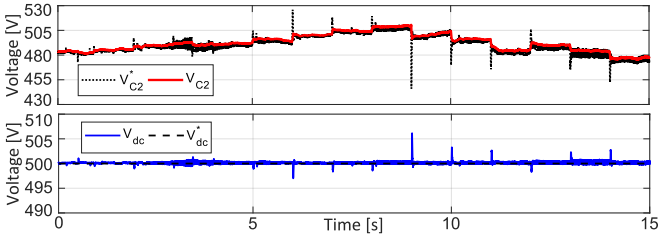

Fig. 5. Voltage V_{C_2} on supercapacitor's converter and DC bus voltage V_{dc}.

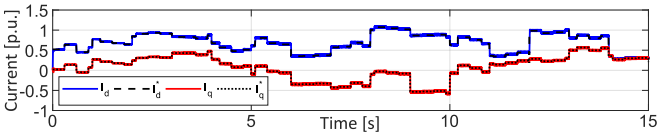

Fig. 6. I_{ld} and I_{lq} currents relating active and reactive power injected into the AC grid.

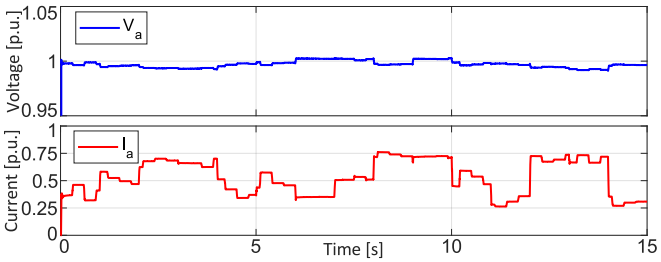

Fig. 7. Rms voltage and current in p.u. on AC grid (phase a).

in Fig. 6 by the controlled currents I_{ld} and I_{lq}.

The MicroGrid is connected to a strong main network with 10 MVA of short-circuit power as mentioned before. Then, voltage and frequency is not the control target of the DC MicroGrid, but just the PQ power supplied for the AC load. Anyway, the injection of active and mainly reactive power to AC side of the grid cause perturbation on the PCC voltage. Thus, rms AC voltage and rms AC current in per unit is depicted in Fig. 7, where power base is $S_{base} = 100\ kVA$ and the voltage base is $V_{base} = 220\ V$. It can be seen that the AC voltage has a good profile with very small variations according to the reactive power injection, which is inside of the grid requirements. The AC current follows the active power demand for AC load as expected.

From simulations is possible to conclude that the DC MicroGrid operates inside of the grid requirements, since the voltage V_{dc} has overshoots smaller than 5% from the nominal value as shown in Fig. 5. Also, the power supplied by the MicroGrid always meet the demanded power from AC load as depicted in Fig. 6. The result is the proper operation of the MicroGrid with a control law that guarantee stability of the entire system.

V. Conclusions

This paper presents a distributed nonlinear control strategy for a grid-connected DC MicroGrid with integration of renewables and energy storage in order to properly supply a local AC load, assuring power flow balance and stabilization in the DC bus voltage of the MicroGrid. The storage system includes a supercapacitor that is controlled to regulate the DC bus voltage dealing with fast-transient disturbances, while a battery provides the power flow balance in a slower piecewise constant profile to save its life-cycle.

The proposed dynamic feedback linearization control assures proper operation of the MicroGrid by satisfying the control targets, where Input to State Stability (ISS) is obtained, then stability of the whole grid is assured. This is an important characteristic that is intended to be exploited in future works for the interconnection of several MicroGrids. The simulation were performed with detailed circuit's level simulations, and the results highlight the control performance of the system, presenting also good transient response and then we can state that proper operation of the system is established.

References

[1] J. J. Justo, F. Mwasilu, J. Lee, and J.-W. Jung, "Ac-microgrids versus dc-microgrids with distributed energy resources: A review," *Renewable and Sustainable Energy Reviews*, vol. 24, pp. 387–405, 2013.

[2] F. Perez, A. Iovine, G. Damm, and P. Ribeiro, "DC microgrid voltage stability by dynamic feedback linearization," in *2018 IEEE International Conference on Industrial Technology (ICIT)*, Feb 2018, pp. 129–134.

[3] R. H. Lasseter, "Smart distribution: Coupled microgrids," *Proceedings of the IEEE*, vol. 99, no. 6, pp. 1074–1082, 2011.

[4] L. E. Zubieta, "Are Microgrids the Future of Energy?: DC Microgrids from Concept to Demonstration to Deployment," *IEEE Electrification Magazine*, vol. 4, no. 2, pp. 37–44, June 2016.

[5] T. Dragicevic, J. C. Vasquez, J. M. Guerrero, and D. Skrlec, "Advanced LVDC Electrical Power Architectures and Microgrids: A step toward a new generation of power distribution networks." *IEEE Electrification Magazine*, vol. 2, no. 1, pp. 54–65, March 2014.

[6] D. Makrygiorgou and A. Alexandridis, "Stability analysis of dc distribution systems with droop-based charge sharing on energy storage devices," *Energies*, vol. 10, no. 4, p. 433, 2017.

[7] F. Perez and G. Damm, "Dc microgrids," in *Microgrids Design and Implementation*. Springer, 2019, pp. 447–475.

[8] A. Martinelli, P. Nahata, and G. Ferrari-Trecate, "Voltage stabilization in mvdc microgrids using passivity-based nonlinear control," in *57th IEEE Annual Conference on Decision and Control (CDC 2018)*, 2018, pp. WeC14–5.

[9] A. Iovine, S. B. Siad, G. Damm, E. De Santis, and M. D. Di Benedetto, "Nonlinear Control of a DC MicroGrid for the Integration of Photovoltaic Panels," *IEEE Transactions on Automation Science and Engineering*, vol. 14, no. 2, pp. 524–535, April 2017.

[10] ——, "Nonlinear control of an AC-connected DC MicroGrid," in *IECON 2016 - 42nd Annual Conference of the IEEE Industrial Electronics Society*, Oct 2016, pp. 4193–4198.

[11] L. Meng, Q. Shafiee, G. F. Trecate, H. Karimi, D. Fulwani, X. Lu, and J. M. Guerrero, "Review on Control of DC Microgrids and Multiple Microgrid Clusters," *IEEE Journal of Emerging and Selected Topics in Power Electronics*, vol. 5, no. 3, pp. 928–948, Sept 2017.

[12] A. Bidram and A. Davoudi, "Hierarchical structure of microgrids control system," *IEEE Transactions on Smart Grid*, vol. 3, no. 4, pp. 1963–1976, 2012.

[13] D. E. Olivares, A. Mehrizi-Sani, A. H. Etemadi, C. A. Caizares, R. Iravani, M. Kazerani, A. H. Hajimiragha, O. Gomis-Bellmunt, M. Saeedifard, R. Palma-Behnke, G. A. Jimnez-Estvez, and N. D. Hatziargyriou, "Trends in microgrid control," *IEEE Transactions on Smart Grid*, vol. 5, no. 4, pp. 1905–1919, July 2014.

[14] R. F. Bastos, T. Dragievi, J. M. Guerrero, and R. Q. Machado, "Decentralized control for renewable DC Microgrid with composite energy storage system and UC voltage restoration connected to the grid," in *IECON 2016 - 42nd Annual Conference of the IEEE Industrial Electronics Society*, Oct 2016, pp. 2016–2021.

[15] N. Pogaku, M. Prodanovic, and T. C. Green, "Modeling, Analysis and Testing of Autonomous Operation of an Inverter-Based Microgrid," *IEEE Transactions on Power Electronics*, vol. 22, no. 2, pp. 613–625, March 2007.

[16] H. K. Khalil, *Nonlinear control*. Prentice Hall, 2014.

[17] A. Iovine, G. Damm, E. De Santis, M. D. Di Benedetto, L. Galai-Dol, and P. Pepe, "Voltage Stabilization in a DC MicroGrid by an ISS-like Lyapunov Function implementing Droop Control," in *ECC 2018 - European Control Conference*, Jun 2018.

[18] E. D. Sontag, "Input to state stability: Basic concepts and results," in *Nonlinear and optimal control theory*. Springer, 2008, pp. 163–220.

[19] K. F. Krommydas and A. T. Alexandridis, "Modular Control Design and Stability Analysis of Isolated PV-Source/Battery-Storage Distributed Generation Systems," *IEEE Journal on Emerging and Selected Topics in Circuits and Systems*, vol. 5, no. 3, pp. 372–382, Sept 2015.

[20] E. D. Sontag and Y. Wang, "On characterizations of the input-to-state stability property," *Systems & Control Letters*, vol. 24, no. 5, pp. 351–359, 1995.